Journal of GeoEngineering, Vol. 17, No. 2, pp. 059-071, June 2022
http://dx.doi.org/10.6310/jog.202206_17(2).1

AXIAL FORCE DEPENDENT PUSHOVER ANALYSIS MODEL FOR LATERALLY LOADED PILES

Jiunn-Shyang Chiou [1*] and Yi-Shao Lin [2]

ABSTRACT

Piles subjected to lateral loads also sustain axial loads, which may influence the flexural property of pile sections. To simulate the effects of axial loading on the pile section in nonlinear pushover analysis, this paper presents a pile model that reflects the distribution of flexural rigidity on the basis of initial axial forces in the pile and the change in plastic hinge properties due to varying axial forces. Based on the moment-curvature curves of pile sections at various axial forces obtained from section analyses, both an effective flexural rigidity-axial force relationship and the axial force dependent plastic hinge properties, including the axial force-effective yield moment interaction curve and normalized moment-plastic curvature curves, are constructed for the model. This model is used to simulate pile load tests in the literature, and reasonable predictions are obtained. Parametric analyses are conducted to examine model performance and the influence of varying axial loads on pile response. The conventional method that considers a constant axial load overestimates the lateral stiffness and strength during compression but underestimates those during tension for a single-pile condition. Regarding a group-pile condition, our proposed model can discern the difference in moment profiles and the development of plastic hinges between the front and back piles.

Key words: Axial loading, lateral loading, moment-curvature curves, pushover analysis, plastic hinges.

1. INTRODUCTION

The seismic design methodology of structures is moving toward performance based design. Designing piles to remain elastic under a large design earthquake level is impractical and costly. Under the performance based design concept, the piles can be designed as limited ductility components and they are allowed to have plastic responses at specified positions to develop ductility for energy dissipation. To perform the ductile design of piles, an essential step is to obtain the capacity curve of the piles through pushover analysis for capturing the complete load and displacement capacities of and the damage development in the piles; the piles are designed to have sufficient strength and ductility, and avoid the occurrence of unfavorable damage and excessive inelastic deformation.

Piles are simultaneously subjected to both axial and lateral loadings. In the common pile design, axial and lateral behaviors are treated independently. Many numerical and experimental studies have been conducted to investigate the combined effect of axial and lateral loads. For example, Anagnostopoulos and Georgiadis (1993) conducted model tests to explore the combined effect of axial and lateral loadings on aluminum close-ended piles. Anagnostopoulos and Georgiadis demonstrated that the lateral load significantly influenced the axial capacity of a pile, whereas the effect of axial loading on the lateral pile response was relatively trivial. Karthigeyan *et al.* (2006) conducted three dimensional finite element numerical analyses to investigate the combined effect of axial and lateral loadings on piles in sand. They revealed that for a short pile in dense sand, the axial loading significantly influenced the lateral pile response (axial loading tended to reduce the lateral displacement); however, on a long pile with pile length-to-diameter ratio > 25, the effect became insignificant. Karthigeyan *et al.* (2007) further conducted three dimensional numerical analyses to explore the lateral response of piles in clay. The influence of axial loading on the lateral response was opposite to that occurring in sand; the axial load tended to increase the lateral displacement. Similarly, the axial loading effect became insignificant for long piles with pile length-to-diameter ratio > 16. Zormpa and Comodrmos (2018) obtained similar findings in their extensive numerical analyses for piles in sand and clay. They also noted that the second-order effect (P-Δ effect where P is the axial force and Δ is the lateral deflection) due to axial load was insignificant unless it occurred under substantial axial loads or lateral displacements.

In the aforementioned studies, the piles were assumed to be elastic. Actually, the properties of pile sections, especially for concrete piles, are also influenced by axial loading. Chien *et al.* (2013) analyzed field load tests on reinforced concrete drilled shafts that had been subjected to a combination of axial and lateral loadings. They found that axial loading changed the pile section properties and further influenced their lateral behavior. Regarding the pile section during compression, axial loading tended to increase flexural rigidity and strength, resulting in a larger lateral capacity. Chiou *et al.* (2012) conducted parametric analyses on the displacement ductility capacity of fixed head piles, finding that although the lateral stiffness and strength of piles could be increased, the lateral displacement ductility capacity was reduced.

Therefore, the axial loading effect on the nonlinearity properties of a pile section must also be considered. To simulate the nonlinear behavior of the pile, the plastic hinge method is commonly used in structural analysis. Chiou *et al.* (2009) developed a distributed plastic hinge method that can effectively capture the development of plastic zones. The method has been used in some

Manuscript received September 20, 2021; revised December 23, 2021; accepted January 9, 2022.
[1*] Associate Professor (corresponding author), Dept. of Civil Engineering, National Taiwan University, No. 1, Sec. 4, Roosevelt Rd., Taipei 10617, Taiwan, R.O.C. (e-mail: jschiou@ntu.edu.tw).
[2] Graduate Student, Dept. of Civil Engineering, National Taiwan University, No. 1, Section 4, Roosevelt Rd., Taipei 10617, Taiwan, R.O.C.

nonlinear pile and pier pushover analyses (Chiou *et al.* 2011; 2019). In the application of this method, a constant axial load along the pile is assumed for determining the moment-curvature curve of the pile section. The method is effective under a constant axial load condition; however, it becomes inefficient when the influence of variable loading is considered. Actually, when piles are subjected to axial loading, the axial force distribution varies along the pile shaft due to skin frictions on the pile, and even for group piles, the pile head axial loads differ at different pile locations and change as lateral displacement increases.

To include the axial loading effect on the nonlinear behavior of the pile section for pushover analysis, in the present study, we propose a pile model to simulate the distribution of flexural rigidity on the basis of initial axial forces in the pile and the change in plastic hinge properties due to varying axial loading. For this model, a series of section analyses is conducted to obtain moment-curvature curves of the pile section under various axial forces, by which an effective flexural rigidity-axial force relationship is constructed and the conventional distributed plastic hinge model is extended into an axial force dependent plastic hinge model by incorporating axial force dependent moment-plastic curvature curves. Nonlinear pushover analyses are conducted to simulate the pile load tests that are available in the literature to demonstrate the applicability of the model. Furthermore, a series of parametric analyses is conducted to investigate the proposed model's performance in nonlinear analyses of laterally loaded single piles and group piles.

2. DISTRIBUTED PLASTIC HINGE MODEL

The plastic hinge model is commonly used in structural analysis to simulate the nonlinear behavior of structural members (Priestley *et al.* 1996). The conventional plastic hinge model consists in placing a concentrated plastic hinge to represent an expected plastic zone that has a fixed plastic hinge length. However, this model is inapplicable to pile foundations because the plastic zone may be changeable under loading and soil nonlinearity. Therefore, Chiou *et al.* (2009) proposed a distributed hinge model for effectively capturing the development of the plastic zone. Unlike the concentrated plastic hinge model, the model does not need to predetermine the precise location of the plastic zone. As illustrated in Fig. 1, many hinges are placed along a potential plastic zone to detect the development of the plastic zone. This model has been applied to piles under various conditions (Chiou *et al.* 2011; Ko *et al.* 2014; Ko and Lin, 2020; He *et al.* 2020) and even to bridge piers (Chiou *et al.* 2019; Chiou and Tsai, 2020). The core of the model is the moment-plastic rotation curve of the distributed plastic hinges. According to Chiou *et al.* (2009), this curve can be deduced based on the moment-curvature curve of the cross-section of the member, as indicated in Fig. 2. The moment-plastic rotation curve is determined by deducing the plastic rotation by using the following equation:

$$\theta_p = \varphi_p l_p = (\varphi - M / EI_e) l_p \quad (1)$$

where θ_p represents the plastic rotation, φ_p represents the plastic curvature, l_p represents the plastic hinge length (which is the tributary length of a hinge, as illustrated in Fig. 1), φ represents the total curvature, M represents the moment, and EI_e represents the effective (elastic) flexural rigidity of the cross-section. For further details of this model, please refer to Chiou *et al.* (2009).

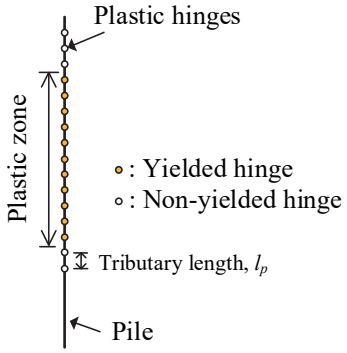

Fig. 1 Distributed plastic hinges on a pile

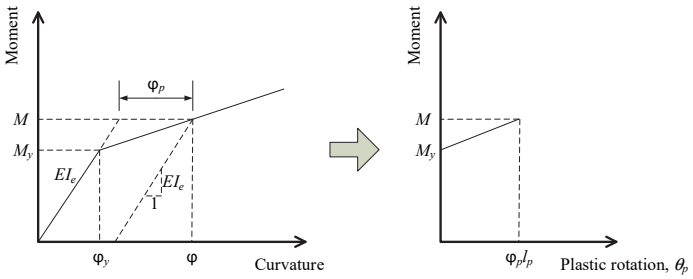

(a) Moment *vs.* curvature (b) Moment *vs.* plastic rotation

Fig. 2 Derivation of moment-plastic rotation curve for distributed plastic hinges (Chiou *et al.* 2009)

When this model is applied to situations in which varying axial loading is considered, the modeling becomes cumbersome because the moment-plastic rotation property will vary with changes in the axial force. Therefore, in the present study, we introduce an axial-moment capacity interaction model (P-M model) to the distributed plastic hinge model to simulate the effects of axial loading.

3. PROPOSED PILE MODEL FOR AXIAL LOADING EFFECTS AND AN AXIAL FORCE DEPENDENT DISTRIBUTED PLASTIC HINGE MODEL

The influence of axial force on the pile section property has two aspects: initial flexural stiffness and the moment capacity curve. To consider these, a pile model that has two components is proposed, as presented in Fig. 3. The basic information for constructing this model comprises a series of moment-curvature curves, obtained based on section analyses that considers various axial forces, as indicated in the dashed lines in Fig. 3(a). These moment-curvature curves are generally simplified as bilinear curves (solid lines), which are defined by effective yield and ultimate points. By applying the curves in Fig. 3(a), the two components of the model are established. The first component is the relationship of effective flexural stiffness varying with the axial force, which is defined using an interaction diagram between effective flexural stiffness EI_e and axial force P, as presented in Fig. 3(b). The second component is the axial force dependent distributed plastic hinge model. The original distributed plastic hinge model is extended to consider the axial force effect

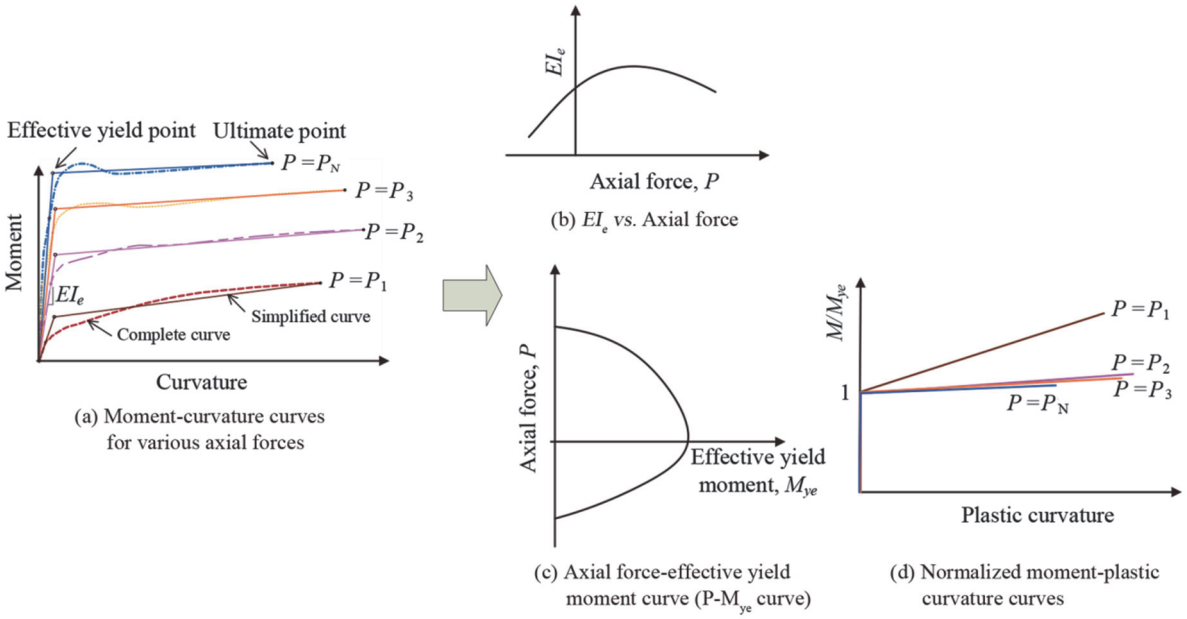

Fig. 3 Determination of parameters of the proposed model

by introducing an axial force-effective yield moment interaction curve (the P-M_{ye} curve) and a set of normalized moment-plastic curvature curves for various axial forces. The P-M_{ye} curve defines the relationship between the effective yield moment M_{ye} and the axial force P based on the curve presented in Fig. 3(c). For each axial force, the normalized moment-plastic curvature curve is determined as illustrated in Fig. 3(d), in which the normalized moment is the moment on the moment-plastic curvature curve that is divided by M_{ye} determined by using the curve presented in Fig. 3(c).

The procedure for applying this model is as follows: First, on the basis of the initial axial force condition, the initial stiffness of the member is determined according to Fig. 3(b). Then, the nonlinear behavior of the moment-plastic curvature relationship can be updated according to various axial force levels by using the curves presented in Figs. 3(c) and 3(d).

4. DEMONSTRATION

4.1 Lateral Load Tests

In the present study, a series of full-scale lateral pile load tests by Chai and Hutchinson (2002) is simulated to evaluate the applicability of our proposed model. According to Chai and Hutchinson (2002), basic information for the tests is summarized as follows: Four full-scale, reinforced concrete piles (Piles 1 ~ 4) of diameter d = 406 mm and length 13.5d were tested under combined axial compressive and cyclic lateral loadings. The piles were tested with aboveground heights of 2d and 6d and in loose and dense dry sand conditions, which are presented in Table 1. A nominal axial compressive force of 445 kN (0.1$f_c'A_g$ where f_c' is the uniaxial compressive strength of the concrete and A_g is the gross sectional area of the pile shaft) was applied to the test piles. The piles had an f_c' of 41 ~ 47 MPa, a longitudinal steel reinforcement ratio ρ_l of 2.1% (7D22), and transverse steel reinforcement ratios ρ_s of 0.57% and 1.06% (Sections 1 and 2, respectively). Sand was compacted in layers around the piles. By using the measurements of cone penetration tests and a shear wave velocity survey, the internal friction angles of soils in the upper 3 m were estimated to be ϕ' = 42° ~ 44° for dense sand and ϕ' = 37° ~ 38° for loose sand, and the relative densities of the test sand, D_r, were estimated to be 94% and 84% for the dense condition (Piles 1 and 3, respectively) and 53% and 59% for the loose condition (Piles 2 and 4, respectively).

Table 1 Test pile conditions

Pile	Aboveground height	Soil condition (Relative density)	Transverse steel ratio
1	812 mm (2d)	Dense (D_r = 94%)	0.57% (Section 1)
2	812 mm (2d)	Loose (D_r = 53%)	0.57% (Section 1)
3	2,436 mm (6d)	Dense (D_r = 84%)	1.06% (Section 2)
4	2,436 mm (6d)	Loose (D_r = 59%)	1.06% (Section 2)

4.2 Simulation

SAP2000 software (Computers and Structures 2017) is used to simulate the four tests. The piles are simulated by beam elements with distributed plastic hinges to account for pile material nonlinearity, and the soil is simulated by nonlinear vertical and horizontal spring elements based on t-z and p-y curves where t is the mobilized soil-pile adhesion at the vertical displacement z and p is the lateral resistance at the lateral deflection y. In the present study, the sand t-z and p-y curves suggested by the American Petroleum Institute (2000) are adopted. The t-z and p-y curves for Piles 1 ~ 4 are presented in Figs. 4 and 5, respectively. Section analysis is conducted to deduce a series of moment-curvature curves under different axial forces, as illustrated in Figs. 6(a) and 6(b) for Sections 1 and 2, respectively. According to the information provided by the moment-curvature curves, the effective flexural stiffness-axial force relationship is established, as displayed in Fig. 7(a). Furthermore, the P-M_{ye} curves and the corresponding moment-plastic curvature curves for several axial forces for the plastic hinges are determined, as displayed in Figs. 7(b) ~ 7(d). In sum, the plastic hinge properties of Sections 1 and 2 are very similar.

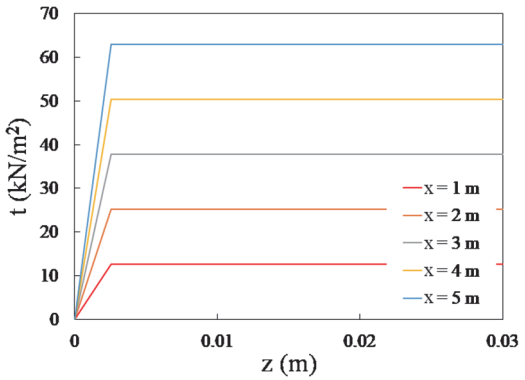

(a) Pile 1 (dense sand, D_r = 94%)

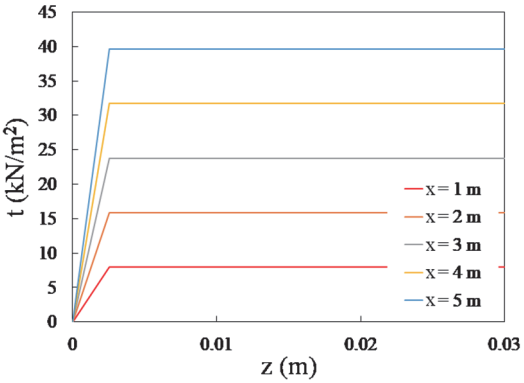

(b) Pile 2 (loose sand, D_r = 53%)

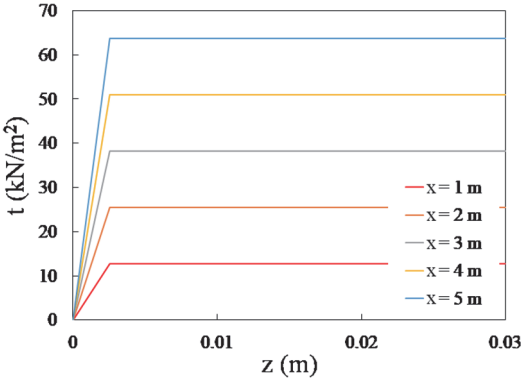

(c) Pile 3 (dense sand, D_r = 84%)

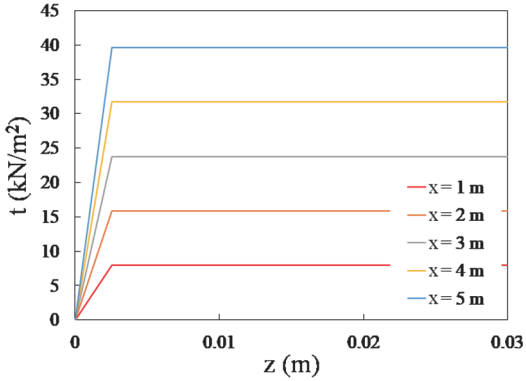

(d) Pile 4 (loose sand, D_r = 59%)

Fig. 4 *t-z* curves of (a) Pile 1; (b) Pile 2; (c) Pile 3; and (d) Pile 4

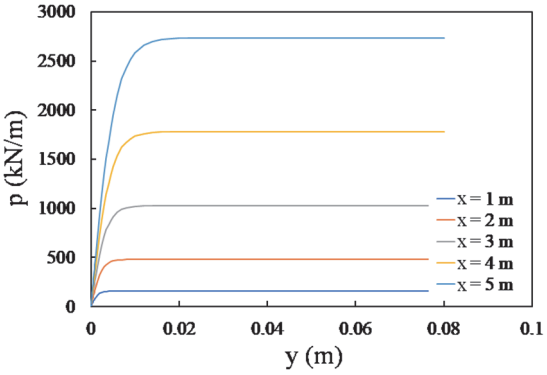

(a) Pile 1 (dense sand, D_r = 94%)

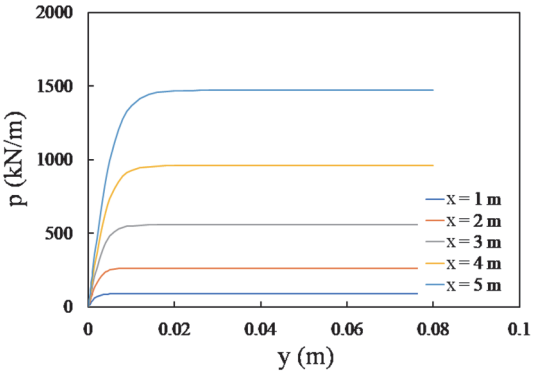

(b) Pile 2 (loose sand, D_r = 53%)

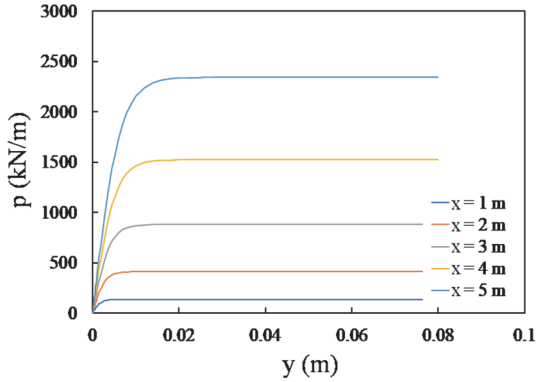

(c) Pile 3 (dense sand, D_r = 84%)

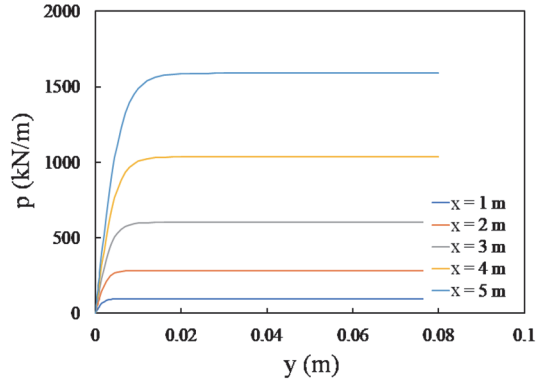

(d) Pile 4 (loose sand, D_r = 59%)

Fig. 5 *p-y* curves of (a) Pile 1; (b) Pile 2; (c) Pile 3; and (d) Pile 4

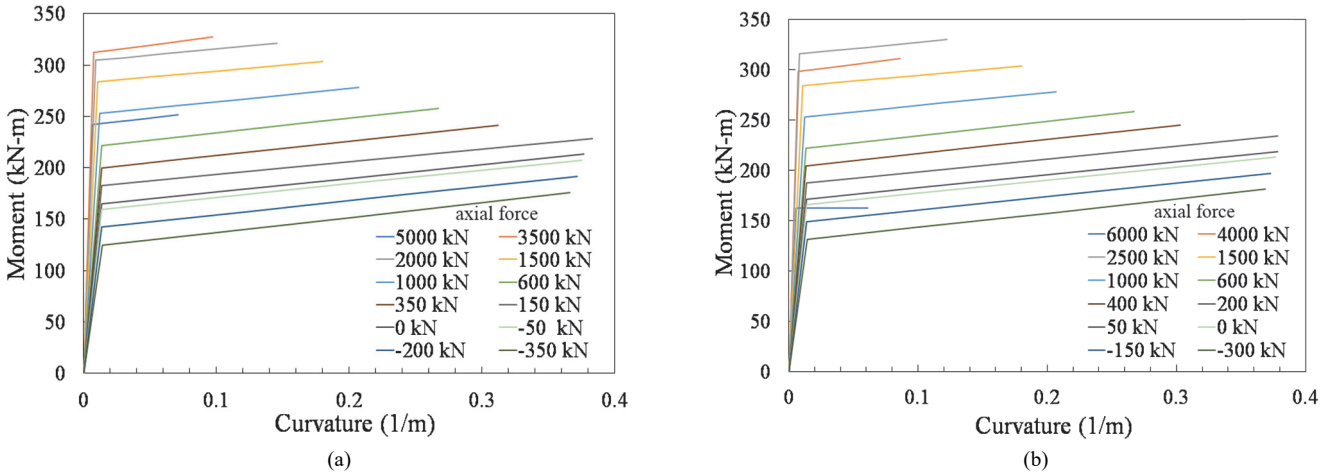

Fig. 6 Bilinear moment-curvature curves for different axial force levels: (a) Section 1 and (b) Section 2

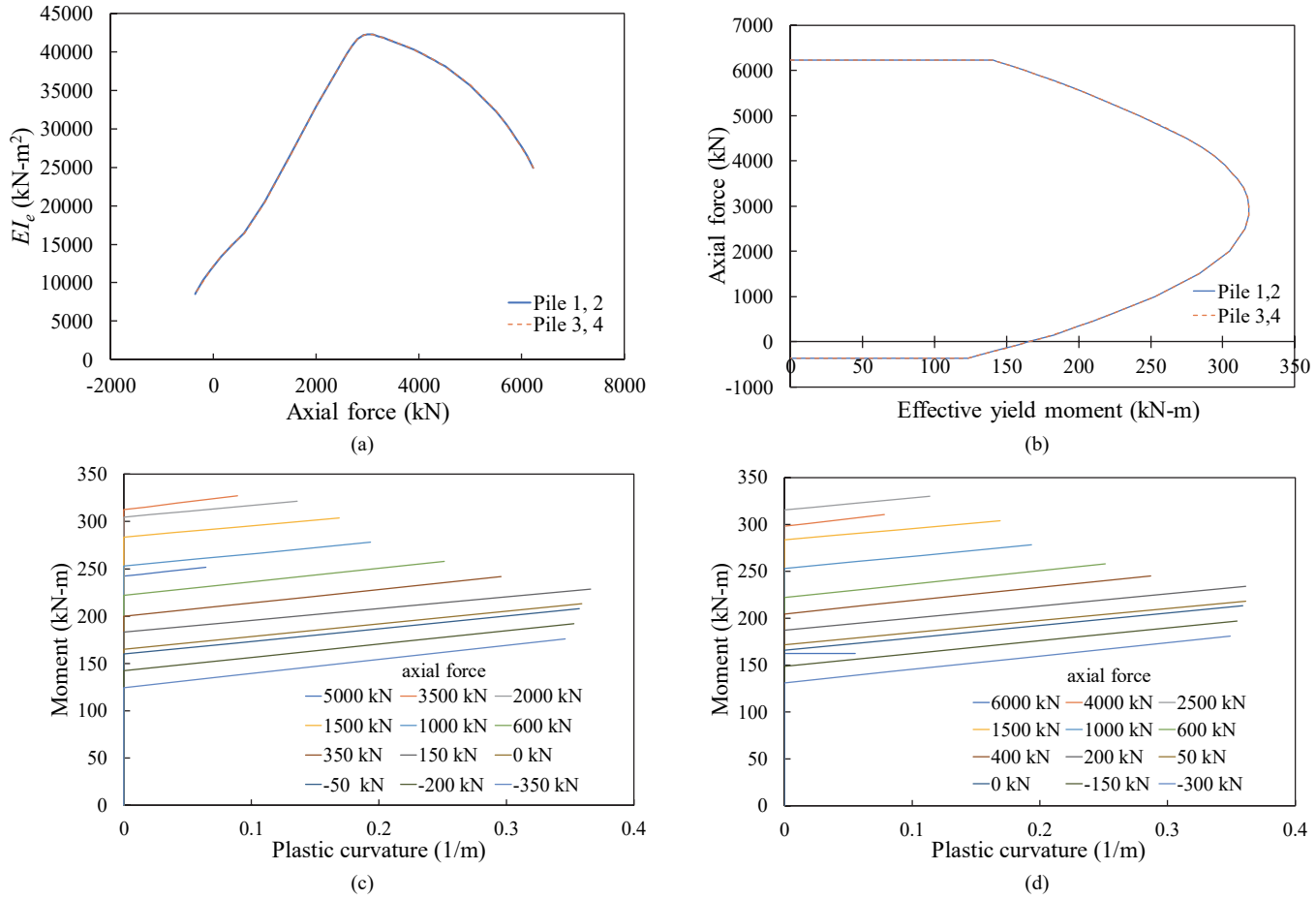

Fig. 7 Axial force dependent properties of Sections 1 and 2: (a) effective flexural rigidity-axial force diagram; (b) axial force-effective yield moment diagram; (c) moment-plastic curvature curves of Section 1; and (d) moment-plastic curvature curves of Section 2

First, the initial flexural stiffness of the pile section in our analyses is determined based on Fig. 7(a). The plastic hinge parameters are set based on Figs. 7(b) ~ 7(d). Figure 8 displays the load-displacement curves of Piles 1 ~ 4. For Piles 1 and 2, the analysis values of initial stiffness are close to the test values, but the maximum lateral strengths are underestimated. For Piles 3 and 4, the initial stiffnesses are slightly underestimated, but the lateral strengths are closely estimated. Despite some deviations in lateral stiffness and strength, the overall trends of the analysis curves are in agreement with those of the test curves, and the post-peak behavior due to the P-Δ effect can be reasonably captured. Because of the P-Δ effect, the lateral displacement keeps increasing despite a reduction in lateral load. Figure 9 displays the predicted and measured curvature profiles of Piles 1 ~ 4. The trends of the curvature profiles as well as the depths of maximum curvature of the analyses are consistent with those of the tests.

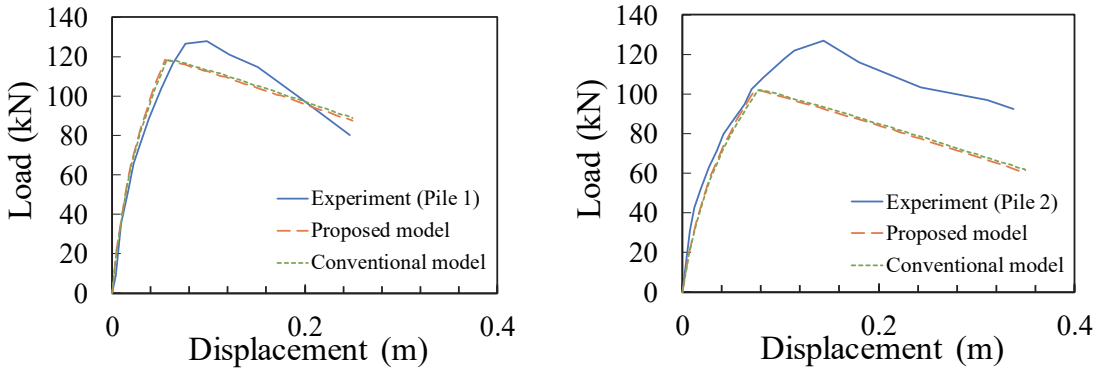

(a) Pile 1 (dense sand, D_r = 94%) (b) Pile 2 (loose sand, D_r = 53%)

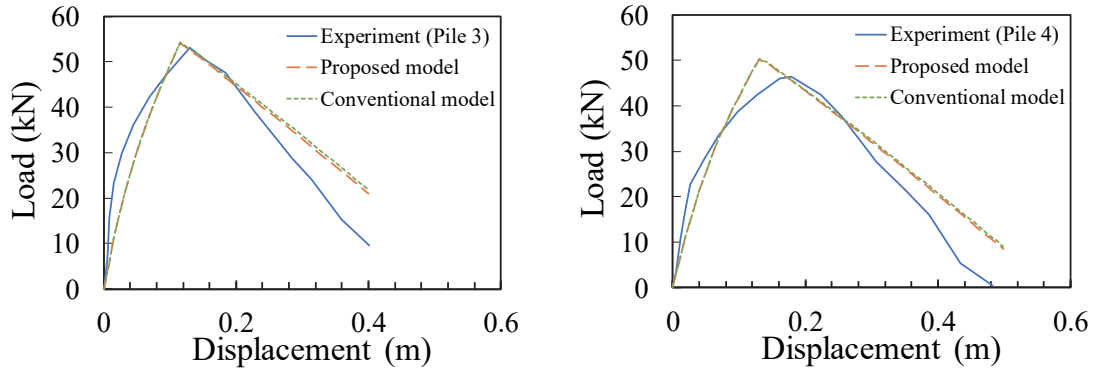

(c) Pile 3 (dense sand, D_r = 84%) (d) Pile 4 (loose sand, D_r = 59%)

Fig. 8 Experimental and predicted load-displacement curves of (a) Pile 1; (b) Pile 2; (c) Pile 3; and (d) Pile 4

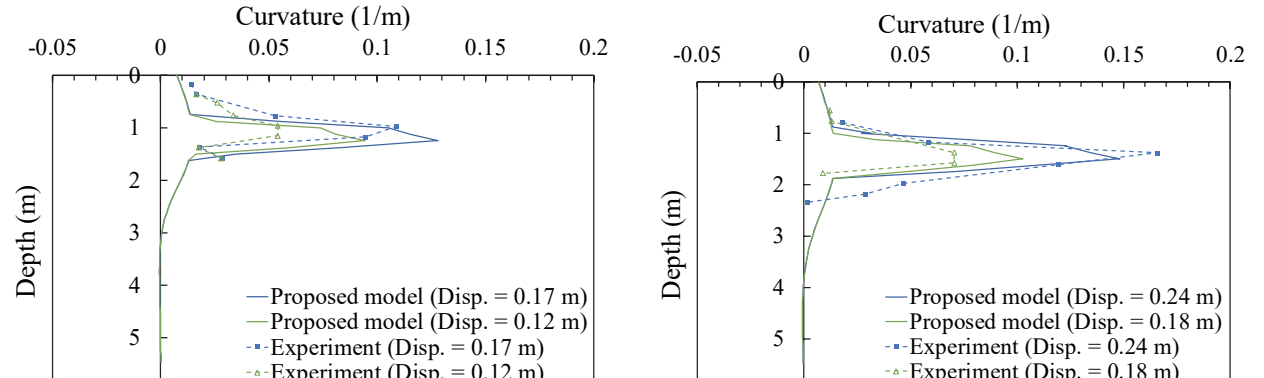

(a) Pile 1 (dense sand, D_r = 94%) (b) Pile 2 (loose sand, D_r = 53%)

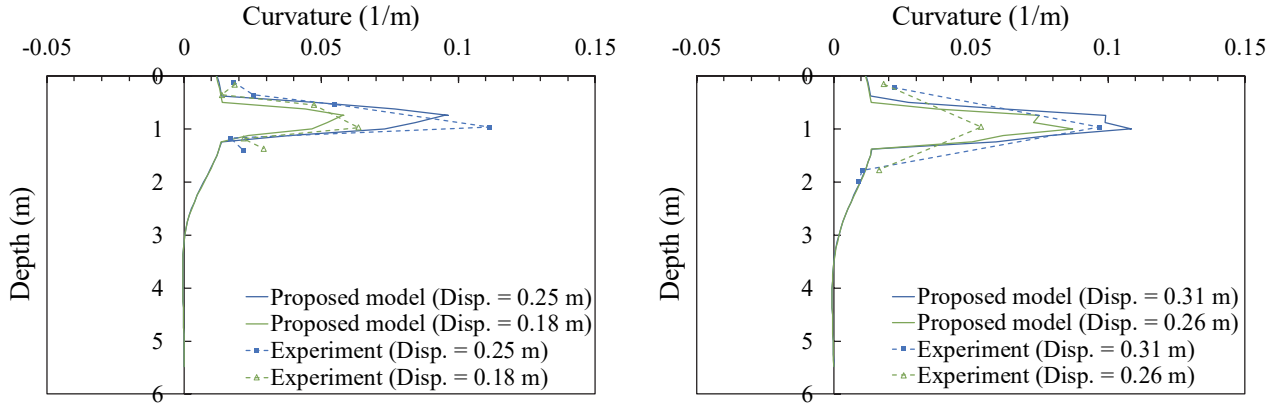

(c) Pile 3 (dense sand, D_r = 84%) (d) Pile 4 (loose sand, D_r = 59%)

Fig. 9 Experimental and predicted curvature profiles of (a) Pile 1; (b) Pile 2; (c) Pile 3; and (d) Pile 4

The conventional distributed hinge model with a specified constant axial load of 445 kN is also applied to simulate these tests for comparison. As illustrated in Fig. 8, the load-displacement curves from the proposed model and the conventional model are very similar because of insignificant variations of axial force profiles with depth. For example, Fig. 10 displays the axial force profiles of Piles 1 ~ 4; the variations of axial force are slight (the maximum axial force difference between the pile head and tip is 49 kN for Pile 1).

5. PARAMETRIC ANALYSES

We further apply the proposed model to conduct parametric analyses for investigating the performance of the proposed model and the influence of axial loading.

When a single pile is subjected to constant vertical pile head loading, the axial force may vary with depth due to skin friction; therefore, the properties of the pile section can change with depth. Furthermore, in a group-pile context, piles at different locations may have different variations in pile head axial loading under lateral loading. Despite complications in the preceding conditions, typical analysis generally considers constant axial loading. In this section, we use our model to conduct a series of parametric analyses to investigate the influence of this simplification on pile responses under single- and group-pile conditions.

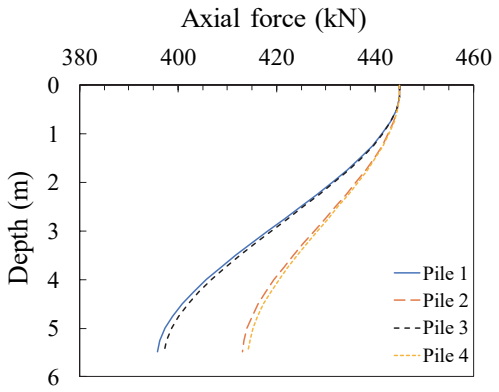

Fig. 10 Axial force profiles of Piles 1 ~ 4

5.1 Single-Pile Condition

For the single-pile condition, a fictitious pile-soil system involving a reinforced concrete long pile with a length of 30 m and a diameter of 1.4 m (the pile length-to-diameter ratio is 21.4) in a homogeneous, cohesive soil is assumed. The structural details of the pile section are a nominal concrete strength f_c' of 27.5 MPa, 20D32 (#10) longitudinal steel, D16 (#5) transverse reinforcement with 100-mm spacing, and a steel yield strength f_y of 412 MPa. The cohesive soil has an undrained shear strength s_u of 60 kPa.

Through section analysis, the moment-curvature curves for different axial forces are obtained, as displayed in Fig. 11(a). According to the aforementioned procedure, the effective flexural rigidity-axial force relationship and plastic hinge properties are determined as presented in Figs. 11(b) ~ 11(d). Figure 12(a) presents the spring model used to simulate different types of soil

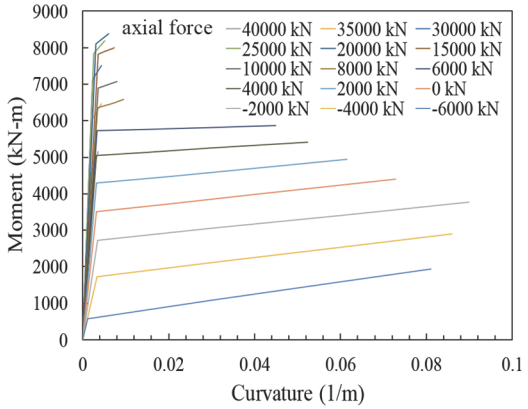

(a) Moment-curvature curves

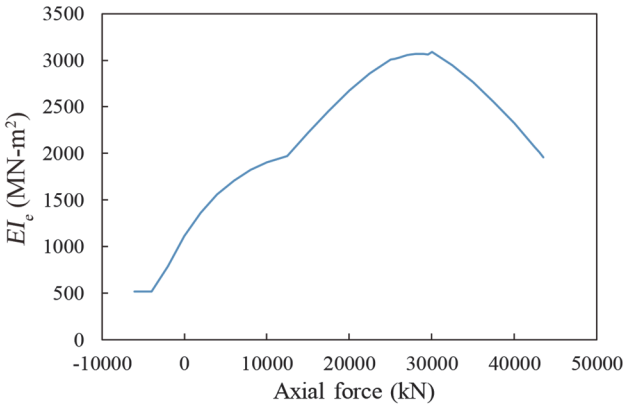

(b) Effective flexural rigidity-axial force diagram

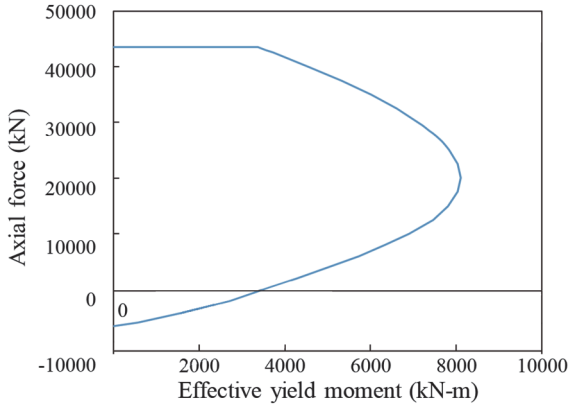

(c) Axial force-effective yield moment diagram

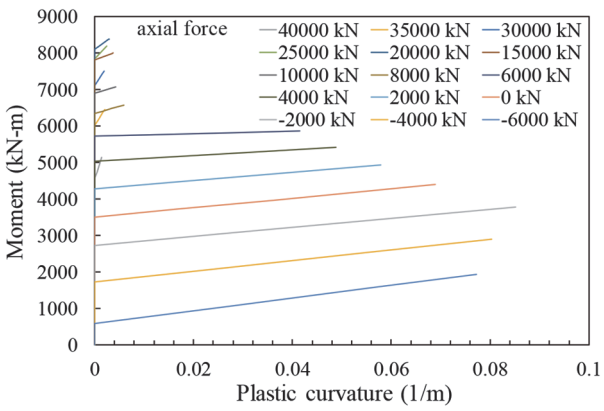

(d) Moment-plastic curvature curves

Fig. 11 Pile section properties

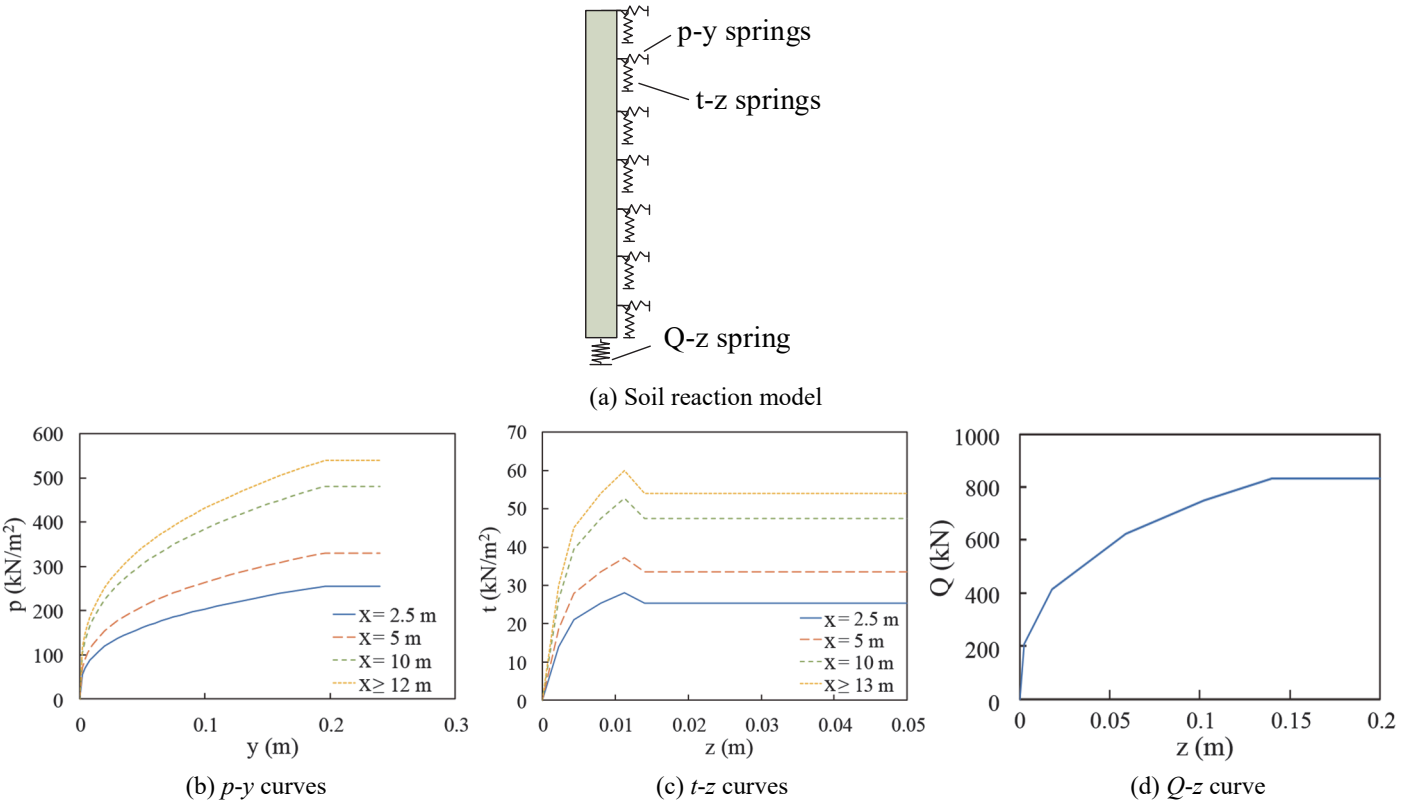

(a) Soil reaction model

(b) *p-y* curves (c) *t-z* curves (d) *Q-z* curve

Fig. 12 Simulation of soil reactions in parametric analyses (s_u = 60 kPa)

reactions on the pile. As presented in Figs 12(b)~12(d), the *p-y* and *t-z* curves for the horizontal and vertical soil reactions, respectively, along the pile and the *Q-z* curve for the base soil reaction, where *Q* is the mobilized end bearing capacity, are determined based on those suggested by American Petroleum Institute (2000). The *p-y*, *t-z*, and *Q-z* curves are generated based on Table 2. For the *p-y* curve, the lateral bearing capacity p_u is computed according to the following equation:

$$p_u = \min\left(3c + \gamma x + J\frac{cx}{D},\ 9c\right) \tag{2}$$

where *c* is the undrained shear strength, γ is the effective unit weight of soil, *J* is the dimensionless empirical constant with values ranging from 0.25 to 0.5 (in the present study, J = 0.5 is used), and *x* is the depth below soil surface.

Table 2 *p-y*, *t-z*, and *Q-z* curves

p-y curve.		*t-z* curve		*Q-z* curve	
y/y_c	p/p_u	z/D	t/t_{max}	z/D	Q/Q_p
0	0.00	0	0	0	0
1	0.50	0.0016	0.3	0.002	0.25
3	0.72	0.0031	0.5	0.013	0.5
8	1.00	0.0057	0.75	0.042	0.75
∞	1.00	0.0080	0.90	0.073	0.90
		0.0100	1.0	0.1	1.0
		0.0200	0.70 ~ 0.90		
		∞	0.70 ~ 0.90		

Note: p_u = ultimate lateral bearing capacity, $y_c = 2.5\varepsilon_c D$, ε_c = strain which occurs at one-half the maximum stress on laboratory undrained compression tests of undisturbed soil samples (ε_c of 0.007 is assumed in the present study), D = pile diameter, t_{max} = maximum unit skin friction capacity, and Q_p = total end bearing.

For the *t-z* curve, the maximum unit skin friction t_{max} is computed according to the following equation:

$$t_{max} = \alpha c \tag{3}$$

where α is a dimensionless factor (≤ 1). It can be computed by the following equation:

$$\begin{aligned} \alpha &= 0.5\psi^{-0.5} \quad \text{for } \psi \le 1.0 \\ \alpha &= 0.5\psi^{-0.25} \quad \text{for } \psi > 1.0 \end{aligned} \tag{4}$$

where $\psi = c/p_0'$ for the point in question and p_0' is the effective overburden pressure at the point in question.

For the *Q-z* curve, the total end bearing Q_p is computed according to the following equation:

$$Q_p = A_p q_p \tag{5}$$

where A_p is the gross base area of pile and q_p is the unit end bearing capacity (= 9*c*).

Figure 13 displays the axial capacity curves under compression and tension. The maximum axial compressive and tensile capacities are approximately 7,000 and 6,500 kN. Accordingly, a compression load of 5,000 kN and a tension load of 3,000 kN are considered for pushover analyses.

Four pile models are used to compare the pushover response of the piles. Model 1 is the proposed model, and it fully considers various initial flexural stiffness and plastic hinge properties with depth (on the basis of the axial forces along the pile). Models 2 ~ 4 are simplified models for different considerations of the axial

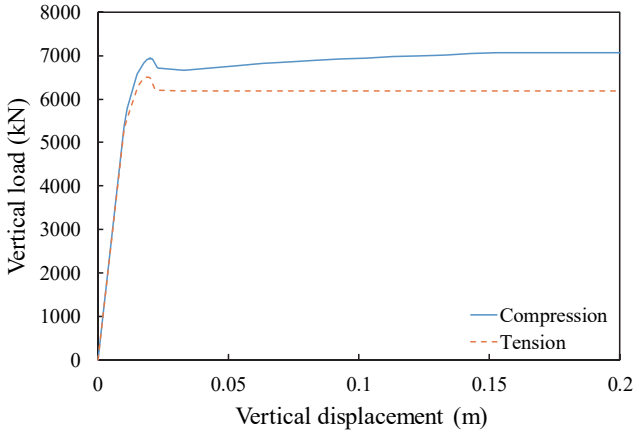

Fig. 13 Axial capacity curves under compression and tension

force effect on the pile section properties. Model 2 considers only the variation of initial flexural stiffness with depth. Model 3 considers only the variation of plastic hinge properties with depth. Model 4 is the conventional model, which adopts constant initial stiffness and plastic hinge properties with depth, on the basis of the pile head load without considering the axial force variation along the pile.

Figure 14(a) presents the load-displacement curves of Models 1 ~ 4 under compression 5,000 kN. For Model 1, Fig. 15(a) displays the axial force profile along the pile shaft, and the associated profiles of flexural rigidity, yield moment, and ultimate moment. The factors of stiffness, yield moment, and ultimate moment between the pile head and the maximum moment depth (approximately 5.5 m) are 0.97, 0.96, and 0.98, respectively. These factors represent the differences of pile section properties within the major deformation zone due to the varying axial force profile; the values less than one represent the decreasing pile section stiffness and strength with depth. This implies that the simplified models will overestimate the stiffness, strength, and ultimate displacement of the pile (the aforementioned values reflect the degree of overestimation). For a small lateral displacement, the four models' curves develop similarly to each other; after a lateral displacement of 0.17 m, the differences among the four curves become substantial. The curve of Model 4 deviates the most from that of Model 1. The difference between Models 3 and 1 is the smallest. The conventional model (Model 4) overestimates the initial stiffness, strength, and ultimate displacement by 0.6%, 2.1%, and 0.2%, respectively. Overall, the development of plastic hinges of the four models is similar. As presented in Fig. 16(a), the maximum plastic zone of the proposed model (Model 1) is located at a depth of 5.5 m with a length of 2.75 m.

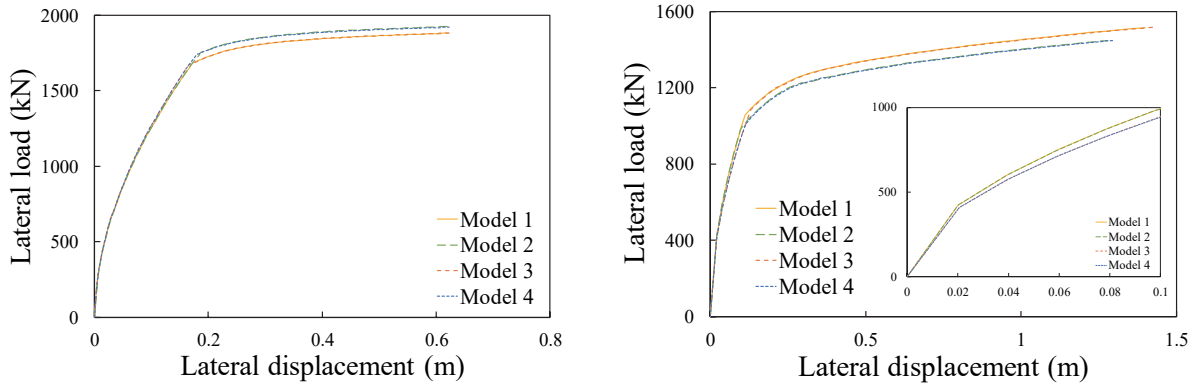

(a) Compression (5,000 kN) (b) Tension (–3,000 kN)

Fig. 14 Pushover curves of Models 1 ~ 4 for s_u = 60 kPa

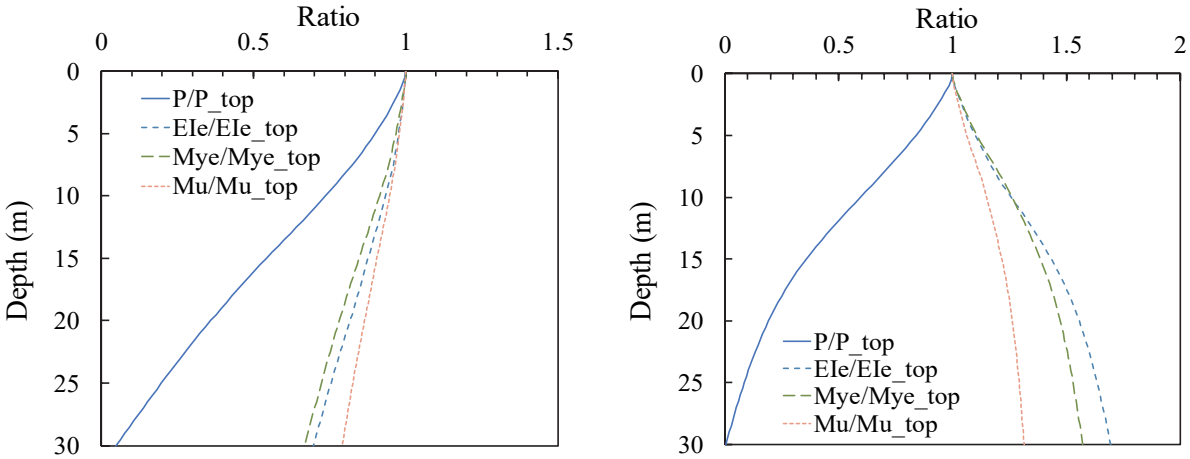

(a) Compression (5,000 kN) (EI_{e_top} = 1.63 × 10^6 kN-m^2, M_{ye_top} = 5,381 kN-m, M_{u_top} = 5,639 kN-m)

(b) Tension (– 3,000 kN) (EI_{e_top} = 6.53 · 10^5 kN-m^2, M_{ye_top} = 2,227 kN-m, M_{u_top} = 3,339 kN-m)

Fig. 15 Profiles of ratios of axial forces, flexural rigidities, and yield and ultimate moments along the pile to those at the pile head

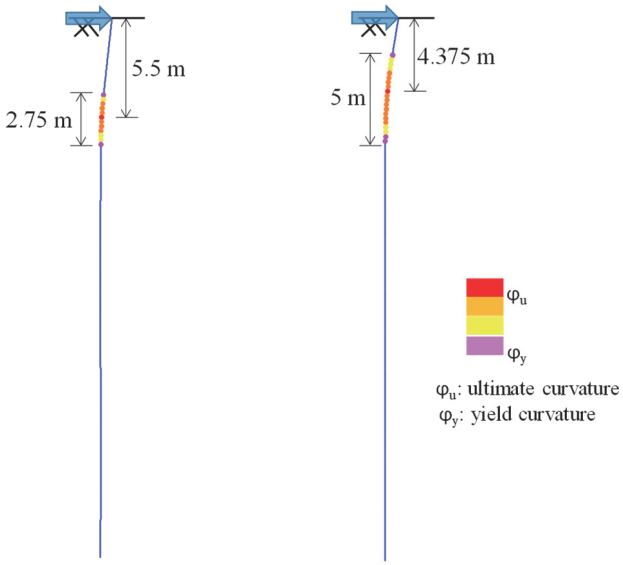

(a) Compression 5,000 kN (b) Tension –3,000 kN

Fig. 16 Development of plastic hinges of the proposed model (Model 1)

Figure 14(b) displays the load-displacement curves for Models 1 ~ 4 under tension 3,000 kN. For Model 1, Fig. 15(b) displays the axial force profile along the pile shaft and the associated profiles of flexural rigidity, yield moment, and ultimate moment. The factors of stiffness, yield moment, and ultimate moment between the pile head and the maximum moment depth (approximately 4.5 m) are 1.09, 1.09, and 1.05, respectively. The values of these factors larger than one represent the increasing pile section stiffness and strength with depth. In contrast to the compression condition, this implies that the simplified models will underestimate the stiffness, strength, and ultimate displacement of the pile (the aforementioned values reflect the degree of underestimation). Compared with the compression condition, the differences in the four model's curves are more significant. The deviation of Model 4's curve from that of Model 1 is the largest, and the differences between the curves of Models 1 and 3 (for varied and constant stiffness profiles, respectively) are the smallest. The conventional model (Model 4) underestimates the initial stiffness, strength, and ultimate displacement by 4.8%, 4.5%, and 7.4%, respectively. The development of plastic hinges of the four models is similar. Figure 16(b) displays the maximum plastic zone of the proposed model (Model 1). The plastic zone of the proposed model (Model 1) is located at a depth of 4.375 m with a plastic hinge length of 5 m. The pile under tension has a shallower but larger plastic zone than that under compression does.

Due to a slight variation in axial force between the pile head and the maximum moment depth, the overall responses of the four models are close. Figure 17 displays the load-displacement curves for Models 1 ~ 4 under compression (5,000 kN) and tension (3,000 kN) for a stratum with a relatively larger strength (s_u = 150 kPa). Compared with the outcome under the previous smaller shear strength condition, the variation of axial force in the pile is more significant; however, the depth of the maximum moment decreases (3.5 m for compression; 3 m for tension). Therefore, the differences in initial stiffness, strength, and ultimate displacement among the four models are also slight under compression. Model 4 overestimates the initial stiffness by 0.6%

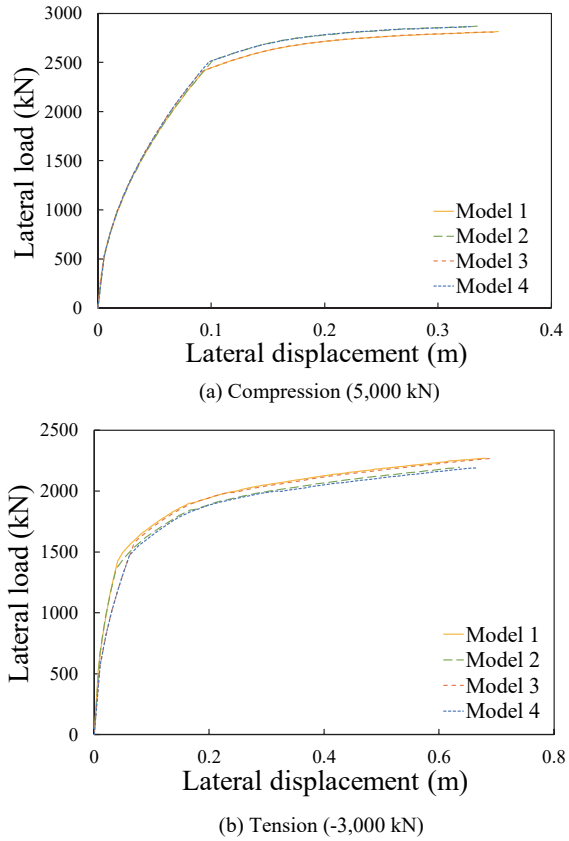

Fig. 17 Pushover curves of Models 1 ~ 4 for s_u = 150 kPa

and strength by 1.8% but underestimates the ultimate displacement by 6.9%. However, the differences are more substantial under tension. The development of the load-displacement curves of the four models also differs. Model 4 underestimates the initial stiffness by 15%, the strength by 3.5%, and the ultimate displacement by 2.4%.

5.2 Group-Pile Condition

Two piles with a rigid cap are assumed for this condition. The pile properties are set equivalent to those adopted for the single-pile condition. The center-to-center spacing of the two piles is assumed to be three times the pile diameter. The effect of group-pile interaction under this group-pile spacing may be significant; however, to clearly observe the effect of varying axial loading on the sectional properties of the group piles, the effect of group-pile interaction is ignored herein. The pile group is subjected to a downward vertical load of 6,000 kN. A conventional approach to determining the properties of a pile section is based on the average vertical load under an assumption that the vertical load is uniformly shared by all piles. However, to consider the different axial loads sustained by the front and back piles during lateral loading, JRA (2012) suggests a rule that the average axial load and zero axial load be adopted, respectively, for piles on the compression and tension sides to determine the pile section properties. However, the main limitation of the JRA method is that when cyclic loading is applied, the piles in compression and tension sides can be reversed for the reversed loading.

In this section, the proposed method (for Model 1), conventional average load method (for Model 4), and JRA method (for

Model 4) are applied to analyze this group-pile problem. Figure 18 presents a comparison of the lateral load-displacement curves of the proposed method, average load method, and JRA method. The JRA method gives a similar initial yield point to that of the proposed method, whereas the average load method overestimates the initial yield point. The average load method underestimates the lateral strength by 0.3% and ultimate displacement by 23%, whereas the JRA method underestimates the lateral strength and ultimate displacement by 5% and 22%, respectively. In addition, the displacement ductility capacity (ultimate displacement divided by yield displacement) predicted by the proposed method is 3.4; the average load method and JRA method underestimate it by 34% and 20%, respectively. The difference in the lateral load-displacement curves is mainly due to the pile head axial load variation between the front and back piles during lateral loading. Figure 19 presents the variations in pile head axial loading with lateral displacement in the proposed method, average load method, and JRA method. As lateral displacement increases (before a lateral cap displacement of approximately 0.12 m), the difference in pile head axial loading between the front and back piles also increases. However, in the proposed method, after a lateral cap displacement of approximately 0.12 m, the difference in pile head axial loading between the front and back piles decreases as the pile head axial loads in the front and back piles decrease.

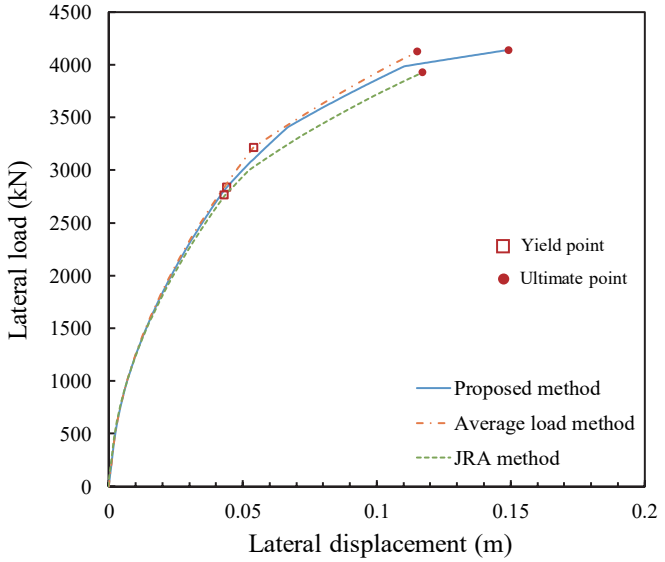

Fig. 18 Group pile pushover curves for the proposed method, average load method, and JRA method

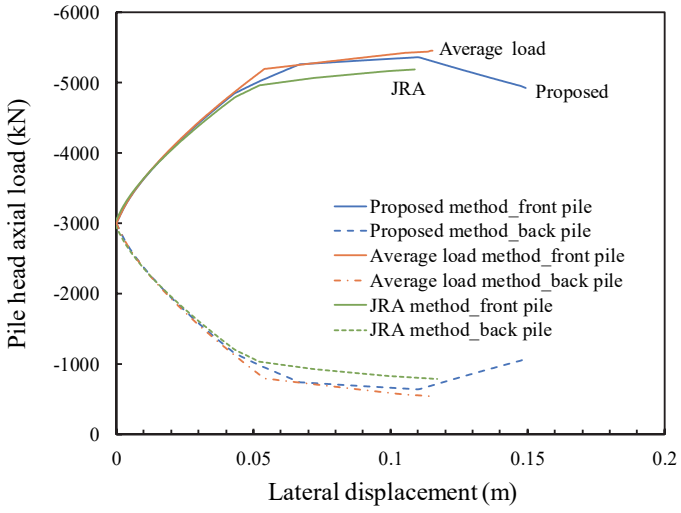

Fig. 19 Variations in pile head axial loading with lateral displacement

The moment distribution and plastic hinge development also differ among the three methods. Figure 20 compares the moment profiles with depth under a cap displacement of 0.115 m in the proposed method, average load method, and JRA method. The average load method cannot distinguish between the compression and tension sides in the group; therefore, the moment profiles for the front and back piles are the same. The JRA method and proposed method can reflect the change in axial load during lateral loading; therefore, the moment profiles for the front and back piles differ. The moment profile of the conventional method is close to that of the front pile of the JRA method. The conventional method tends to overestimate the pile head moment in the back pile, whereas the JRA method tends to underestimate the in-ground maximum moment in the back pile. Figure 21 compares the development of plastic hinges under a cap displacement

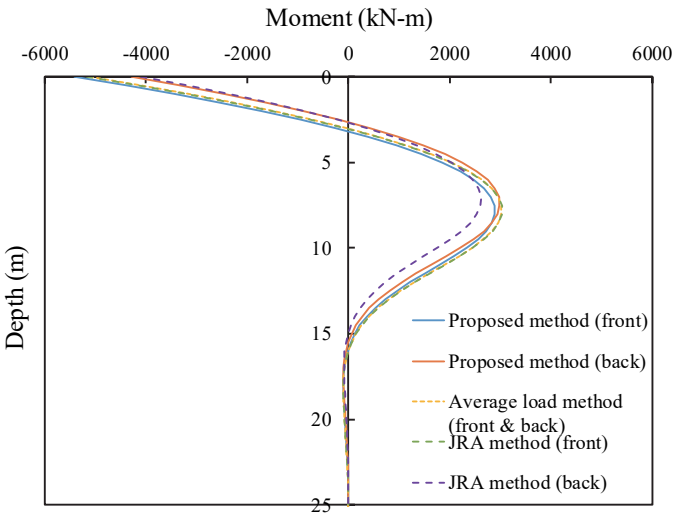

Fig. 20 Moment profiles (cap displacement of 0.115 m)

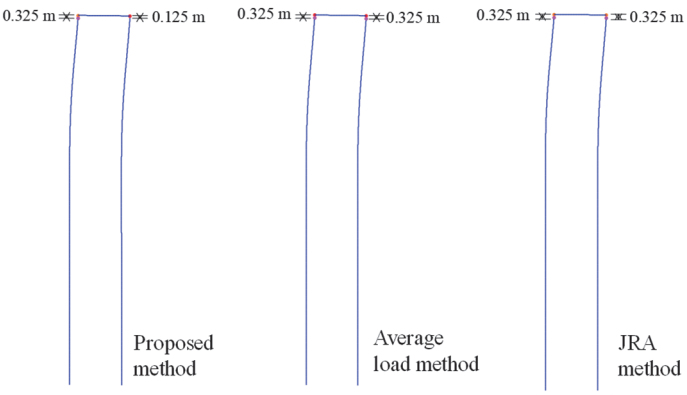

Fig. 21 Development of plastic hinges (cap displacement of 0.115 m)

of 0.115 m under the three methods. In contrast to the single-pile condition, plastic hinging for the group-pile condition occurs at the pile head because the pile head is restrained from rotation by the cap. The pile head plastic zone is generally small. The development of plastic hinges is the same for the front and back piles in the conventional and JRA methods but is different from that of the proposed method. Furthermore, the conventional method cannot reflect the earlier yielding and a larger plastic zone in the back pile than in the front pile.

In the above analyses, the effect of group-pile interaction is ignored. In addition to the abovementioned influence due to varying axial loads, the effect of group-pile interaction may further cause a reduction in the lateral stiffness and strength of group piles.

6. DISCUSSION

The differences in the pile responses among Models 1 ~ 4 for single piles under compression are generally small. The axial force effect on the lateral pile stiffness and ultimate displacement is relatively slight, but the effect on the strength is greater. By contrast, for single piles under tension, the differences in pile responses among the four models are much larger, and the axial force effect on the lateral pile stiffness can be larger.

The ratios of the lateral strengths of Models 4 and 1 are close to those of the ultimate moments at the pile head and at the maximum moment depth of the pile. For a pile with a significant variation of axial force within its maximum moment depth, the difference between the proposed model and conventional model are more pronounced, especially for a pile under tension. When piles are in compression or when the post-yield pile behavior is the focus, the proposed model (Model 1) can be further simplified to Model 3, which is under the assumption that pile-section stiffness is constant along the depth and equivalent to the pile-head sectional stiffness under the pile head axial load and uses the distributed plastic hinges with the P-M model to account for the variation in flexural strength and curvature capacity due to the variations in axial force along the pile.

Regarding the group-pile condition, because the pile head loads and their differences in the front and back piles vary with lateral loading, the lateral load-displacement curves, as well as the moment profiles and development of plastic hinges, differ under the proposed method and the conventional average load method.

7. CONCLUSIONS

We proposed a pile model for pushover analysis to consider the axial force effects on the stiffness and strength of a pile section. By using the moment-curvature curves under various axial forces obtained from section analysis, we generated an effective flexural rigidity-axial force diagram and created an axial force-effective yield moment diagram with a set of normalized moment-plastic curvature curves to set the properties of the distributed plastic hinges. To demonstrate the model's applicability, we used it to simulate field pile load tests that have been reported in the literature. Additionally, a series of parametric analyses was conducted to investigate the performance of the proposed model in single- and group-pile conditions by comparing its results with those of the simplified models with different degrees of simplification of the axial force effects. When piles are in compression or when the focus is on nonlinear pile behavior, the proposed model can be simplified to only consider the axial force dependent plastic hinge model. The strength of the proposed model is its applicability to group-pile conditions for simulating the influence of varying pile head loads on the front and back piles under lateral loading and on the different developments of plastic zones in the piles.

FUNDING

This work is funded by the Ministry of Science and Technology, Taiwan (Grant no. MOST 108-2628-E-002-004-MY3) and the National Taiwan University, Taiwan (Grant no. NTU-CC-110L891305).

DATA AVAILABILITY

Some or all data, models, or code that support the findings of this study are available from the corresponding author upon reasonable request.

CONFLICT OF INTEREST STATEMENT

The authors declare that they have no known conflict of interests or personal relationships that could have appeared to influence the work reported in this paper.

REFERENCES

American Petroleum Institute (2000). *API Recommended Practice for Planning, Designing, and Constructing Fixed Offshore Platforms — Working Stress Design*. Report RP-2A-WSD, API Publishing Services, Washington, DC.

Anagnostopoulos, C. and Georgladis, M. (1994). "Interaction of axial and lateral pile responses." *Journal of Geotechnical and Geoenvironmental Engineering*, ASCE, **119**(4), 793-798. https://doi.org/10.1061/(ASCE)0733-9410(1993)119:4(793)

Chai, Y. H. and Hutchinson, T.C. (2002). "Flexural strength and ductility characteristics of extended pile-shafts. II: Experimental study." *Journal of Structural Engineering*, ASCE, **128**(5), 595-602. https://doi.org/10.1061/(ASCE)0733-9445(2002)128:5(586)

Chien, C.J., Lin, S.S., Yang, C.C., and Liao, J.C. (2013). "Lateral performance of drilled shafts due to combined lateral and axial loading." *Journal of Mechanics*, **29**(4), 685-693. https://doi.org/10.1017/jmech.2013.55

Chiou, J.S., Yang, H.H., and Chen, C.H. (2009). "Use of plastic hinge model in nonlinear pushover analysis of a pile." *Journal of Geotechnical and Geoenvironmental Engineering*, ASCE, **135**(9), 1341-1346. https://doi.org/10.1061/(ASCE)GT.1943-5606.0000015

Chiou, J.S., Chiang, C.H., Yang, H.H., and Hsu, S.Y. (2011). "Developing the fragility curves for a pile-supported wharf." *Soil Dynamics and Earthquake Engineering*, **31**(5-6), 830-840. https://doi.org/10.1016/j.soildyn.2011.01.011

Chiou, J.S., Tsai, Y.C., and Chen, C.H. (2012). "Investigating influencing factors on the ductility capacity of a fixed-head reinforced concrete pile in homogeneous clay." *Journal of*

Mechanics, **28**(3), 489-498. https://doi.org/10.1017/jmech.2012.58

Chiou, J.S., Jheng, Y.W., and Hung, H.H. (2019). "Numerical simulation of bridge piers with spread footings under earthquake excitation." *Earthquakes and Structures*, **16**(6), 691-704. https://doi.org/10.12989/eas.2019.16.6.691

Chiou, J.S. and Tsai, C.C. (2020). "Analysis of in situ bridge columns with exposed caisson foundations in a gravel stratum under lateral loading." *Advances in Structural Engineering*, **23**(3), 424-437. https://doi.org/10.1177/1369433219872441

Computers and Structures, Inc. (2017). *SAP2000*. *Integrated Software for Structural Analysis and Design*. Computer Program, Computers & Structures, Inc., Berkeley, CA, USA.

He, L.G., Hung, H.H., Chuang, C.Y., and Huang, C.W. (2020). "Seismic assessments for scoured bridges with pile foundations." *Engineering Structures*, **211**(15), 110454. https://doi.org/10.1016/j.engstruct.2020.110454

Japan Road Association (JRA). (2012). *Design Specifications for Highway Bridges —IV: Substructures* (in Japanese).

Karthigeyan, S., Ramakrishna, V.V.G.S., and Rajsgopal, K. (2006). "Influence of vertical load on the lateral response of piles in sand." *Computers and Geotechnics*, **33**, 121-131. https://doi.org/10.1016/j.compgeo.2005.12.002

Karthigeyan, S., Ramakrishna, V.V.G.S., and Rajsgopal, K. (2007). "Numerical investigation of the effect of vertical load on the lateral response of piles." *Journal of Geotechnical and Geoenvironmental Engineering*, ASCE, **133**(5), 512-521. https://doi.org/10.1061/(ASCE)1090-0241(2007)133:5(512)

Ko, Y.Y., Chiou, J.S., Tsai, Y.C., Chen, C.H., Wang, H., and Wang. C.Y. (2014). "An evaluation on flood resistant capacity of scoured bridges." *Journal of Performance of Constructed Facilities*, ASCE, **28**(1), 61-75. https://doi.org/10.1061/(ASCE)CF.1943-5509.0000381

Ko, Y.Y. and Lin, Y.Y. (2020). "A comparison of simplified modeling approaches for performance assessment of piles subjected to lateral spreading of liquefied ground." *Geofluids*, Article ID 8812564. https://doi.org/10.1155/2020/8812564

Priestley, M.J.N., Seible, F., and Calvi, G.M. (1996). *Seismic Design and Retrofit of Bridges*. Wiley-Interscience, New York. https://doi.org/10.1002/9780470172858

Zormpa, T.E. and Comodromos, E.M. (2018). "Numerical evaluation of pile response under combined lateral and axial loading." *Geotechnical and Geologic Engineering*, **36**, 793-811. https://doi.org/10.1007/s10706-017-0354-1